

File ID uvapub:85597
Filename 329486.pdf
Version final

SOURCE (OR PART OF THE FOLLOWING SOURCE):

Type article
Title Nonlinear reaction coordinate analysis in the reweighted path ensemble
Author(s) W. Lechner, J. Rogal, J. Juraszek, B. Ensing, P.G. Bolhuis
Faculty FNWI: Van 't Hoff Institute for Molecular Sciences (HIMS)
Year 2010

FULL BIBLIOGRAPHIC DETAILS:

<http://hdl.handle.net/11245/1.329486>

Copyright

It is not permitted to download or to forward/distribute the text or part of it without the consent of the author(s) and/or copyright holder(s), other than for strictly personal, individual use, unless the work is under an open content licence (like Creative Commons).

Nonlinear reaction coordinate analysis in the reweighted path ensemble

Wolfgang Lechner,¹ Jutta Rogal,² Jarek Juraszek,³ Bernd Ensing,¹ and Peter G. Bolhuis^{1,a)}

¹van 't Hoff Institute for Molecular Sciences, University of Amsterdam, Nieuwe Achtergracht 166, 1018WV Amsterdam, The Netherlands

²Interdisciplinary Centre for Advanced Materials Simulation (ICAMS), Ruhr University Bochum, 44780 Bochum, Germany

³Spanish National Cancer Research Centre (CNIO), Melchor Fernandez Almagro 3, 28029 Madrid, Spain

(Received 29 April 2010; accepted 2 September 2010; published online 1 November 2010)

We present a flexible nonlinear reaction coordinate analysis method for the transition path ensemble based on the likelihood maximization approach developed by Peters and Trout [J. Chem. Phys. **125**, 054108 (2006)]. By parametrizing the reaction coordinate by a string of images in a collective variable space, we can optimize the likelihood that the string correctly models the committor data obtained from a path sampling simulation. The collective variable space with the maximum likelihood is considered to contain the best description of the reaction. The use of the reweighted path ensemble [J. Rogal *et al.*, J. Chem. Phys. **133**, 174109 (2010)] allows a complete reaction coordinate description from the initial to the final state. We illustrate the method on a z-shaped two-dimensional potential. While developed for use with path sampling, this analysis method can also be applied to regular molecular dynamics trajectories. © 2010 American Institute of Physics. [doi:10.1063/1.3491818]

I. INTRODUCTION

Numerical studies of rare events in high-dimensional complex systems, such as chemical reactions in solution or protein conformational changes, are often conducted with biased simulations methods such as umbrella sampling,¹ blue moon sampling,² metadynamics,³ etc. These methods bias the systems along a predefined reaction coordinate in order to sample the rarely visited parts of phase space: the transition state (TS) region. A major drawback of such biasing methods is that they all require in some way a description of the relevant reaction coordinate (RC). Instead, one would like to extract a reaction coordinate from the simulation itself. In fact, such a procedure is often used. Visual inspection of preliminary molecular dynamics (MD) or Monte Carlo (MC) simulations suggests some tentative relevant collective variables for the rare event. The subsequent use of these collective variables in the rare event sampling method then gives rise to a free energy profile or landscape in terms of these variables and the prospective transition state (ensemble). However, there is no guarantee that this particular choice of the reaction coordinate will lead to meaningful results. A poorly chosen RC might then result in a completely wrong mechanism and a statistically unmeasurable rate constant.⁴ A systematic way of finding and extracting a reaction coordinate would therefore be very useful. In this paper, we are concerned with such a systematic reaction coordinate extraction for rare events. Any systematic method would require the sampling of unbiased reactive trajectories, i.e., without prior knowledge of the RC. The transition path sampling (TPS) method⁵ was designed to harvest a collection

of unbiased dynamical trajectories that connect the initial with the final state. The resulting transition path ensemble provides the basis for the RC analysis.

At the heart of the RC analysis is the concept of the commitment probability or committor p_B . This quantity is defined for a certain high-dimensional configuration \mathbf{r} as the probability that a trajectory initialized with random momenta from this configuration reaches the final state B before the initial state A . The dividing surface in the configuration space is then given by those configurations that have equal commitment probability for either state, i.e., $p_B=p_A=0.5$. Because the transition path ensemble sampled by TPS contains all true dynamical paths connecting the two states, we can label those configurations in the path ensemble with committor 0.5 as transition states, thus forming a transition state ensemble. Moreover, the committor function $p_B(\mathbf{r})$ is the best possible reaction coordinate, as it represents a progress variable that smoothly changes from 0 to 1 and at each step of the reaction/transition gives the probability to complete the reaction.⁶ The transition path theory (TPT) provides the framework for a complete description of the statistical properties of the transition path ensemble in terms of the committor function and the equilibrium distribution, and gives expressions for the path probability density, the probability current, as well as the reaction rate.^{6,7} Still, the committor function itself does not immediately give physical insight into the reaction mechanism, as it is a function of a high-dimensional configuration space \mathbf{r} . The task of the RC analysis is thus to approximate the committor using a low dimensional parametrization in terms of collective variables, such as distances between atoms or angles, that can yield insight in the reaction.

A straightforward way to test whether a prospective collective variable q parametrizes the committor was put for-

^{a)}Electronic mail: p.g.bolhuis@uva.nl.

ward in Ref. 8 in order to find a pertinent reaction coordinate for isomerization in alanine dipeptide. The approach consists of generating by a constraint method (e.g., umbrella sampling¹ or blue moon sampling²) an ensemble of configurations \mathbf{r}_q for the value of q characterized by the location of the transition state, and then computing the committor values $p_B(\mathbf{r}_q)$ for this ensemble. The distribution of the committor $P(p_B(r))$ can evaluate the quality of the prospective reaction coordinate q . If the distribution is peaked around 0.5, then q is a qualitatively good RC, and if it is bimodal, it is poor.

This committor analysis, although powerful, is computationally very expensive because for each prospective RC, an ensemble of configurations and their committor values must be evaluated. A more efficient approach was proposed by Ma and Dinner in Ref. 9. Instead of computing the committor many times for different prospective RCs, they computed it once for many different configurations, chosen such that the p_B values were approximately uniformly distributed. One way of doing so is to use the transition path ensemble obtained by TPS. For each configuration treated, the computed committor value is stored in a database, together with a long list of collective variables. Using a genetic neural network (GNN), one can search for combinations of collective variables that best fit the committor data. While already much more efficient than the original committor analysis, the GNN approach is still expensive due to the explicit computation of the committor data on top of the TPS simulations.

Best and Hummer^{10,11} developed an efficient reaction coordinate analysis technique by combining the equilibrium probability distribution with path ensemble distributions. In this method, the conditional probability $p(\text{TP}|r)$ for a configuration with a certain value of the reaction coordinate r to lie on a transition path TP connecting the initial and final states is expressed by the Bayesian relation $p(\text{TP}|r) = p(r|\text{TP})p(\text{TP})/p_{\text{eq}}(r)$. Here, $p_{\text{eq}}(r)$ denotes the equilibrium distribution as a function of r , $p(r|\text{TP})$ is the distribution of configurations with a certain r visited along transition pathways in the TPS ensemble, and the factor $p(\text{TP})$ is the overall likelihood to be on a transition path.¹¹ $p(\text{TP}|r)$ is large for r corresponding to configurations that are part of transition pathways but are rarely visited in an equilibrium simulation. Thus, the maximum of $p(\text{TP}|r)$ corresponds to transition states, i.e., the configurations with the maximum probability that trajectories going through them are reactive.¹⁰ For diffusive dynamics, $p(\text{TP}|r) = 2p_B(r)(1-p_B(r))$, where $p_B(r)$ is the committor averaged over all configurations with r . For a good reaction coordinate, all transition states approximately have the same value of r and thus, $p(\text{TP}|r)$ should be peaked around the transition state value of r . In contrast, if r is a poor reaction coordinate, the lack of correlation between r and $p(\text{TP}|r)$ will render this distribution featureless. In this sense, the Best–Hummer approach can determine the quality of a chosen reaction coordinate. The method requires an accurate equilibrium distribution in the transition region, which might be difficult to obtain. In addition, in Ref. 6 it is argued that $p(r|\text{TP})$ is not sufficient for describing the RC and that the probability current as following from TPT is more informative about the reaction mechanism.

Peters and Trout^{12,13} developed a likelihood maximiza-

tion (LM) method that eliminated any committor computation, but only uses data from the shooting points of a TPS simulation. They realized that the TPS shooting move could be interpreted as an instance of a committor computation with only one trajectory. Hence, the estimate for p_B is zero or unity. Nevertheless, based on the TPS shooting point ensemble data, one can search for the best model reaction coordinate that reproduces the data using a likelihood maximization. To obtain unbiased instances of a committor computation, Peters and Trout adjusted the regular shooting move into “aimless shooting,” such that it produced randomized velocities and at the same time remained in the neighborhood of the transition state region, where the commitment probability $P(\text{TP}|x)$ is close to its maximum. Subsequently, the aimless shooting point data are fitted to a reaction coordinate composed of a linear combination of tentative collective variables. Screening all possible combinations of candidate collective variables for the maximum likelihood yields the best reaction coordinate model for the given data. Peters and Trout show that this approach works and applied it to the nucleation in the Ising model.¹² The method has also been used for finding reaction coordinates in protein folding.^{14,15} Escobedo¹⁶ and co-workers developed a similar method to find reaction coordinates in the forward flux sampling method based on least-squares fitting of the commitment probability.

The LM procedure by Peters and Trout is powerful, but still suffers from two drawbacks. (1) It only gives information around the TS region of the reaction, whereas in some processes information on the entire reaction is required to understand the complex mechanism. (2) A nonlinear approximation to the RC is usually more difficult to find and optimize than a linear one. In this paper, we address these two points simultaneously by allowing for a nonlinear description of the reaction coordinate that completely describes the reaction from the initial to the final state. Note that by nonlinearity, we mean not the nonlinearity of the collective variables themselves (previous works often use nonlinear collective variables such as angles^{12,17,18}), but the nonlinear correlation between these collective variables describing the entire reaction. This nonlinear description is based on ideas from the string method as developed by Vanden-Eijnden and co-workers.^{19,20} (We also note that Peters and Trout already suggest to use a string optimization procedure,¹² although not for the reaction coordinate optimization.)

We will illustrate our new approach on the z-potential (see Ref. 21 and Fig. 6). This two-dimensional (2D) potential has two stable states separated by one barrier. Hence, diffusive (Langevin) dynamics in this potential will exhibit classical two state behavior with a well-defined rate constant. However, the pathways connecting the two stable states follow, on average, a pattern resembling the letter z. First, the system has to move into the x direction before it can move into the y direction, but then it has also to move back in the x direction along the diagonal, cross the barrier, and, when on the other side, it has to transverse once more into the (positive) x direction. This convoluted reaction pathway is easy to understand when plotting the potential in the x,y plane. However, when the potential is projected onto the x

coordinate only, the reaction coordinate is less clear. The free energy as a function of x only still gives a two state potential, but when pushing the system along the x axis starting from the initial state, it will not reach the final state unless pushed very hard. A large degree of hysteresis is the result and the true transition state will be avoided. Similarly, when only y is known and the system is pushed into that direction, the TS region will be avoided and hysteresis is the result. In fact, only by taking into account the correlation between the x and y parameters, and defining the RC to follow the z shape as well, will allow a smooth transition from the initial to final state and vice versa without hysteresis. Clearly, such a RC must be nonlinear. This simple 2D model hence is a good test case to develop nonlinear RC methods.

The LM scheme by Peters and Trout requires the use of the aimless shooting algorithm. However, for complex diffusive problems, we would like to be able to use the *one-way* shooting method with flexible path length²² for the RC analysis. Here, we show that using the shooting point ensemble as obtained from the one-way shooting algorithm leads to a bad fit of the committor p_B when using a linear description of the RC. We also show that this linear fit improves by cutting the shooting point ensemble such that only the data close to the TS region are selected. Cutting the shooting point ensemble indeed improves the reaction coordinate, but is somewhat arbitrary. In fact, the aimless shooting procedure naturally restricts the shooting point ensemble to the phase space region close to the TS. The improvement of the RC only applies to the transition state region. As mentioned above, any linear RC will never be able to fit the entire mechanism in the z -potential. Although the LM procedure also takes into account nonlinear fits, we propose the use of a fully flexible RC in the form of a string of images. Such a string is a discrete representation of the reaction coordinate. Using the LM optimization for the string then leads to the best nonlinear model for the RC. To compute the likelihood corresponding to each string requires a projection method from the shooting points onto the string. We use a geometrical procedure that was introduced in Ref. 21, as well as a Voronoi-like construction inspired by the work on the string method.²⁰

An optimization of the string in phase space regions far away from the transition state requires very accurate committor data in those regions. Such data are not available from a regular shooting point ensemble because shots that are far away from the TS region will most likely end in one of the two states. The committor values for the other state are hence estimated to be close to zero. As the likelihood maximization sums over the logarithm of these numbers, these data are very inaccurate. However, such accurate committor values are available from the unbiased path ensemble, which can be estimated by the reweighting scheme introduced in Ref. 21. The reweighted path ensemble (RPE) gives accurate committor values along the entire transition (see also Appendix B). Using the RPE instead of the shooting point ensemble, we are able to optimize the string description of the RC over the whole phase space from the initial to the final region. Moreover, using the same arguments as Peters and Trout,¹² we can

find the collective variable space in which the string description provides the best model for the reaction coordinate.

The paper is organized as follows. We introduce the theoretical background and the methodology in Sec. II. Next, we show in Sec. III B that the one-way shooting point ensemble does not lead to a proper linear RC description for the z -potential. In Sec. III C we apply our new string method to the RPE data obtained by replica exchange transition interface sampling (RETIS) of the z -potential. We optimize the number of string images and show that a 2D reaction coordinate is vastly superior to a one-dimensional (1D) description of the same data. We end with concluding remarks.

II. METHODS

A. Likelihood maximization

The basis of the likelihood maximization method for reaction coordinates by Peters and Trout is to use the set of shooting points from aimless shooting and their final destination (A or B) as instances of a committor computation. By projection onto a RC defined as a function of some collective variables, one can compute the likelihood to observe the data (i.e., the sampled shooting points). Optimizing this likelihood for different combinations of collective variables then yields the best model for the reaction coordinate with respect to the given data.

In the first step, a set of shooting points from a TPS simulation is collected. A shooting point \mathbf{x} is the random starting point for TPS trajectories during the shooting move.^{5,12,13} Here, $\mathbf{x}=\{\mathbf{r}^N, \mathbf{p}^N\}$ denotes a point in a phase space, with \mathbf{r} and \mathbf{p} as the coordinates and momenta of the N -particle system at a certain time. For each shooting point \mathbf{x} , one can define a RC that depends (linearly) on n collective variables q as

$$r(\mathbf{x}) = \sum_i^n \alpha_i q_i(\mathbf{x}) + \alpha_0, \quad (1)$$

where the α_i coefficients are to be optimized. The collective variables q_i are predefined/chosen functions that are candidates for important ingredients in the RC, such as radius of gyration, root mean square deviation, distances, angles, etc. The committor can then be modeled as a simple tanh function

$$p_B(r(\mathbf{x})) = \frac{1}{2}(1 + \tanh(r(\mathbf{x}))). \quad (2)$$

For diffusive dynamics, the likelihood for the shooting point data is^{11,12}

$$\mathcal{L} = \prod_{\mathbf{x}_i \rightarrow B} p_B(r(\mathbf{x}_i)) \prod_{\mathbf{x}_i \rightarrow A} p_A(r(\mathbf{x}_i)), \quad (3)$$

where the committor p_A for state A is simply $p_A(r)=1-p_B(r)$. The first product runs over trial shooting points that lead to B and the second over shooting points that lead to A . It is more convenient to express the likelihood as a logarithm

$$\ln \mathcal{L} = \sum_{\mathbf{x}_i \rightarrow B} \ln p_B(r(\mathbf{x}_i)) + \sum_{\mathbf{x}_i \rightarrow A} \ln p_A(r(\mathbf{x}_i)). \quad (4)$$

When used only with the shooting points close to the TS region, as resulting from the aimless shooting method, the best option is to assume linear reaction coordinates.¹²

The different path sampling shooting algorithms give rise to different shooting point distributions. In Appendix B we show how these distributions depend on the different algorithms.

B. Approximating the RC by a string

While the method of Peters and Trout in principle allows for nonlinear RCs, in practice, linear approximations are often used because the shooting point ensemble remains close to the TS region due to the aimless shooting algorithm. When the process of interest is very complex and consists of multiple sequential steps, a nonlinear reaction coordinate might be better to describe the reaction. Also, for TPS methods that do not employ the aimless shooting algorithm, the shooting point ensemble will be more diffuse and contain instances of shots far away from the TS region.

A flexible way of incorporating nonlinearity is to represent the reaction coordinate by a string of points (just as in the string method¹⁹). This string consists of M reference points in the q space

$$\mathbf{S} = \{\mathbf{s}_0, \mathbf{s}_1, \dots, \mathbf{s}_M\}, \quad (5)$$

where \mathbf{s} denotes the d -dimensional position in the space of the current choice of collective variables space $\mathbf{q} = \{q_1, q_2, \dots, q_d\}$. The string connects the stable states A and B and represents the reaction coordinate. Now any $6N$ -dimensional point \mathbf{x} has to be assigned a position $\sigma(\mathbf{S}(\mathbf{q}(\mathbf{x})))$ along the string, where $\sigma \in [0, 1]$. We employ two different projection methods. The first is a geometrical projection method onto the string, presented in Ref. 21, which yields a continuous number σ for each point \mathbf{x} . The σ number then has to be mapped to the RC itself by a function $r=f(\sigma)$, where $f(\sigma)$ could, for instance, be a simple (monotonic) polynomial (cubic) spline function that translates between σ and r . Thus the assignment of an RC value to a phase point \mathbf{x} reads

$$r(\mathbf{x}) = f(\sigma(\mathbf{S}(\mathbf{q}(\mathbf{x}))). \quad (6)$$

The second projection method used in this paper is a Voronoi construction, where each phase point is assigned to the closest two string images, with a piecewise linear interpolation to obtain a continuous σ value. This σ value is then translated into the RC r by a simple piecewise (monotonic) linear interpolation. For simplicity, we can combine the q to σ and the σ to r mappings into one, as is schematically shown in Fig. 1. The string in a two-dimensional plane is assigned a value of r at each image. The end points of the string are fixed in x, y space. In this way, any point in the x, y plane can be projected on the closest linear line segment of the string and thus translated to a value of r . Note that a choice of dynamically coupled collective variables might render these projection methods problematic as in that case, the isocommittor surfaces are no longer orthogonal to the string.^{23,24}

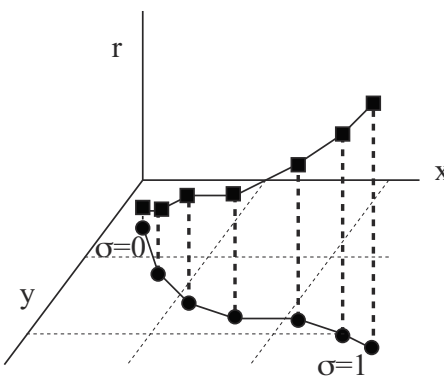


FIG. 1. An example of how the coordinate space can be mapped onto a string using a Voronoi projection method plus piecewise linear interpolation. Each string point has an r value translating the continuous σ value into a reaction coordinate value.

The effect of the choice of units can be removed by including an additional scaling factor in the optimization or, e.g., by following the approach of Ref. 20. Both the string image positions \mathbf{S} and their corresponding r values can be adjusted in the likelihood optimization. This amounts to $M(d+1) - 2d$ variables to be optimized (the $2d$ term arises because the end points are fixed). In the case of a 2D string ($d=2$), this amounts to $3M-4$ variables. For the optimization, a simulated annealing scheme is used (see Appendix A).

The idea of the string optimization approach is that we would get information about the RC not only close to the transition state where $p_B=0.5$, but also close to the stable states. As an example, we can look at the z-potential, where a linear RC approximation clearly cannot describe the entire pathway.

C. The reweighted path ensemble from RETIS

The proposed string method approach will fail when only shooting points are used, as was done in Ref. 12, because shooting points close to the stable states hardly exist. Even if in the one-way shooting point ensemble there are shooting points close to a stable state, they are nearly always of one kind (A or B) (see Sec. III B 2). Hence, the estimate for the p_B function for extreme values of the reaction coordinate (when p_B is either almost 0 or almost 1) is very inaccurate. One way to improve the statistics of shooting points close to the initial and final state is to realize that not only the shooting points themselves can be seen as committor computation, but, in principle, all time slices on the TPS pathways can be considered a realization of a committor computation. This follows from the fact that for stochastic dynamics, each phase point \mathbf{x} has a well-defined committor value $p_B(\mathbf{x})$. Therefore, one could include all configurations in the path ensemble in the analysis. To avoid biasing the committor distributions, this path ensemble should be equal to the unbiased complete path ensemble, i.e., containing all possible paths starting from A and all paths starting from B . A schematic view of this unbiased path ensemble is given in Fig. 2. The unbiased path ensemble can be used to accurately estimate the p_B values even at extreme values of the RC.

One way of obtaining the unbiased path ensemble is a very long straightforward MD simulation. Of course, such a

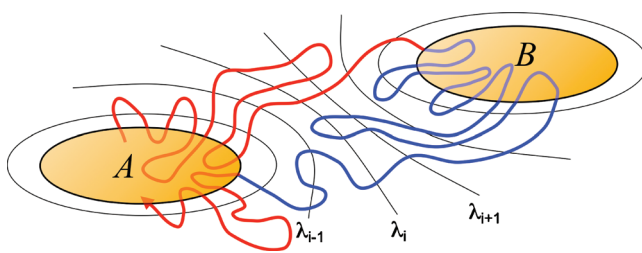


FIG. 2. Cartoon of the unbiased path ensemble in the context of transition interface sampling. The red and blue curves denote the path ensemble for *A* and *B*, respectively.

naive calculation of the unbiased path ensemble is suffering from the very rare event problem that we are trying to solve. However, it is possible to compute this complete path ensemble within the transition interface sampling²⁵ (TIS) methodology by reweighting the interface ensembles using the weighted histogram analysis method (WHAM),²⁶ as was shown in Ref. 21. Here, we briefly review the method. TIS introduces $n+1$ nonintersecting interfaces between *A* and *B* described by a progress variable $\lambda(\mathbf{x})$ which is a function of the phase point \mathbf{x} . The n interfaces are defined by an ordered sequence $\lambda_0, \lambda_1, \dots, \lambda_n$, where the first interface λ_0 is the boundary of state *A* and the last one (λ_n) is identical to the boundary of state *B*. The TIS path ensemble consists of trajectories $\mathbf{x}^L = \{\mathbf{x}_0, \mathbf{x}_1, \dots, \mathbf{x}_L\}$, an ordered sequence of phase space points \mathbf{x} . The time-step between these points, or time slices, is Δt , resulting in a total time duration of the path of $T=L\Delta t$. The paths start in *A* and either end in *B* or return to *A*, provided that they have crossed a certain interface λ_i . Defining the region of phase space beyond interface i by $\Lambda_i^+ = \{\mathbf{x} : \lambda(\mathbf{x}) > \lambda_i\}$, the TIS path probability is

$$\mathcal{P}_{A\Lambda_i^+}[\mathbf{x}^L] = \tilde{h}_i[\mathbf{x}^L] \rho(\mathbf{x}_0) \prod_{i=0}^{L-1} p(\mathbf{x}_i \rightarrow \mathbf{x}_{i+1}) / Z_{A\Lambda_i^+}, \quad (7)$$

where $\rho(\mathbf{x})$ denotes the steady state distribution, e.g., the canonical distribution, $p(\mathbf{x} \rightarrow \mathbf{y})$ represents the Markovian probability to go from a state \mathbf{x} to \mathbf{y} within one time interval Δt , and the normalizing factor $Z_{A\Lambda_i^+}$ is defined by $\int d\mathbf{x} \mathcal{P}_{A\Lambda_i^+}[\mathbf{x}^L] = 1$. The indicator function $\tilde{h}_i[\mathbf{x}^L] = 1$ for paths that begin in *A*, end in *A* or *B*, and cross λ_i and zero otherwise. The TIS path ensemble can be sampled using the regular shooting algorithm. Sampling efficiency can be improved by employing replica exchange (RETIS).^{27,28}

The TIS path ensembles can be reweighted using a WHAM analysis of the crossing histograms.²¹ By defining an expression similar to Eq. (7) for the reverse process $B \rightarrow A$, the reweighted path ensemble for both the forward and reverse process is

$$\mathcal{P}[\mathbf{x}^L] = c_A \sum_{j=1}^{n-1} \mathcal{P}_{A\Lambda_j^+}[\mathbf{x}^L] W^A[\mathbf{x}^L] + c_B \sum_{j=1}^{n-1} \mathcal{P}_{B\Lambda_j^+}[\mathbf{x}^L] W^B[\mathbf{x}^L], \quad (8)$$

where the function $W^A[\mathbf{x}^L] = \sum_{i=1}^{n-1} \bar{w}_i^A \theta(\lambda_{\max}[\mathbf{x}^L] - \lambda_i) \theta(\lambda_{i+1} - \lambda_{\max}[\mathbf{x}^L])$ selects the correct interface weight for each path \mathbf{x}^L based on the maximum λ along the path. Similarly, $W^B[\mathbf{x}^L] = \sum_{i=1}^{n-1} \bar{w}_i^B \theta(\lambda_{\min}[\mathbf{x}^L] - \lambda_i) \theta(\lambda_{i+1} - \lambda_{\min}[\mathbf{x}^L])$ selects the

weights for paths from *B* based on the minimum λ along the path. The weights \bar{w}_i^A and \bar{w}_i^B can be obtained from WHAM analysis²⁶ of the forward and reverse crossing probability histograms, respectively.²¹ The unknown constants c_A and c_B follow from matching the AB and BA histograms for overlapping interfaces (note that for the complete path ensemble, we would need to include the additional RETIS ensembles $P_{\Lambda_1^-}$ and $P_{\Lambda_{n-1}^+}$. For more information we refer to Ref. 21).

D. Likelihood maximization using the RPE

We can employ the reweighted path ensemble in the string algorithm described above. All stored phase points \mathbf{x} of each pathway \mathbf{x}^L are assigned a weight $\omega = W(\mathbf{x})$. All weights are normalized such that the lowest weight in the ensemble is unity. Assuming diffusive dynamics,¹² the total likelihood for the RPE is then

$$\mathcal{L} = \prod_{\mathbf{x}_i \rightarrow B} p_B(r(\mathbf{x}_i))^{\omega_i} \prod_{\mathbf{x}_i \rightarrow A} p_A(r(\mathbf{x}_i))^{\omega_i} \quad (9)$$

because each point is occurring exactly ω_i times in the ensemble. The logarithmic likelihood is then

$$\ln \mathcal{L} = \sum_{\mathbf{x}_i \rightarrow B} \omega_i \ln p_B(r(\mathbf{x}_i)) + \sum_{\mathbf{x}_i \rightarrow A} \omega_i \ln p_A(r(\mathbf{x}_i)). \quad (10)$$

This likelihood can be maximized by modifying the positions of the string images \mathbf{S} until convergence. To avoid getting trapped in local maxima, we employ a Monte Carlo annealing method to optimize the string (see Appendix A).

E. Optimizing the number of string images

Up to now we have assumed that the number of string images is fixed. However, we cannot be certain in advance that we have the optimal number. Increasing the number of string images might provide a better description of the RC, but also increases the number of variables. If the number of variables becomes larger, fitting of the data becomes easier. The Bayesian information criterion (BIC) can determine the optimal number of variables.²⁹ According to this criterion, the following expression should be maximized:

$$C_{\text{BIC}} = \ln \mathcal{L} - \frac{1}{2} n_v \ln N_d, \quad (11)$$

where N_d is the number of data points (shooting points in our case). As we are employing the RPE, this number is $N_d = \sum_{i=0}^{N_f} \omega_i$, where N_f is the number of time slices in the path ensemble. n_v is the number of variables in the description of the model. In our case $n_v = dM + n_\sigma$, with d as the dimension of the collective variable space, M as the number of string images, and n_σ as the number of points used in the $r(\sigma)$ mapping. For the case of the simultaneous string and RC mapping (cf. Fig. 1) and fixed string end points $n_v = (d+1) \times (M-2) + 2 = 3M - 4$.

F. What is the best collective variable space?

Optimizing the likelihood for one set of collective variables by the string method is not sufficient. The idea of the LM is to provide a quantitative way to distinguish between different sets of collective variables. In the method devel-

oped by Peters and Trout,¹² this is done by starting with a list of collective variables and computing the likelihood for each of these. Then the likelihoods for all linear combinations of two collective variables are calculated. When the optimal likelihood $\ln \mathcal{L}$ increases by an amount of $0.5 \ln N_d$, this combination is deemed a significantly better reaction coordinate than the best 1D collective variable. Subsequently, one can consider all combinations of three collective variables, etc.

We can apply a similar procedure for our string RC optimization using the criterion of Eq. (11). We first compute the maximum likelihood for all candidate collective variables by projecting the data points onto each collective variable. Optimizing the σ to r mapping then provides directly the RC model that best describes the committor without any string optimization. Next, we test all combination of two different collective variables by optimizing strings in these 2D spaces. When the maximal C_{BIC} is greater than the 1D value, we regard the string reaction coordinate to be significantly better than any of the 1D collective variables. Again, the extension to more dimensions is straightforward, although the number of combinations to test rises steeply. Note that while the committor itself is the optimal reaction coordinate and is indeed a “one-dimensional” variable, our aim is to identify the smallest set of collective variables that permit to parametrize this function accurately.

III. RESULTS AND DISCUSSION

A. The potential

In this work, we employ a two-dimensional model system for which the potential is given by

$$\begin{aligned} V(x,y) = & \frac{x^4 + y^4}{20480} - 3e^{-0.01(x+5)^2 - 0.2(y+5)^2} \\ & - 3e^{-0.01(x-5)^2 - 0.2(y-5)^2}, \\ & + \frac{5e^{-0.2(x+3(y-3))^2}}{1+e^{-x-3}} + \frac{5e^{-0.2(x+3(y+3))^2}}{1+e^{x-3}}, \\ & + 3e^{-0.01(x^2+y^2)}. \end{aligned} \quad (12)$$

This potential is visualized in Fig. 6. It has two stable states: one at $(-7.2, -5.1)$ and at $(7.2, 5.1)$. These two minima are separated by a barrier in the shape of the letter s, due to the presence of two high potential ridges. At the origin the potential is $V=4.28k_B T$ above the minima. The minimum energy pathway is indicated, and roughly follows the reversed z shape.

The system consists of a single particle evolving according to Langevin dynamics on this potential. For details on the algorithm see, e.g., Ref. 5. The A and B regions are defined as ellipsoidal regions around the minima (x_m, y_m) as $\{x, y \mid (x-x_m)^2 + \frac{1}{16}(y-y_m)^2 < R^2\}$. The radius is set to $R=0.5$.

B. Committor surface and the linear LM approximation

1. Numerical committor evaluation

An exhaustive numerical evaluation of the committor surface can be performed for this simple system by shooting

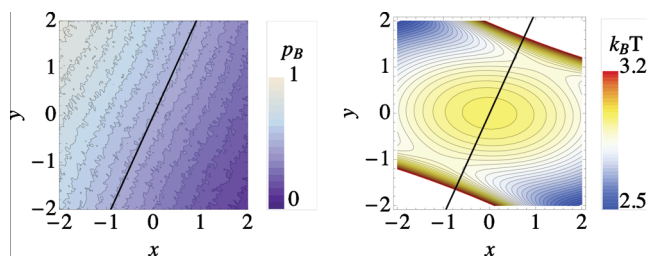


FIG. 3. Left: A contour plot of a numerical evaluation of the committor surface $p_B(x,y)$ around the transition state. The contours are separated by 0.05. The solid line depicts the dividing surface $p_B=0.5$. Right: The dividing surface plotted on the potential surface around the TS region. Note that the dividing surface does not pass through the two saddle points.

many trajectories from each x,y point around the transition state with random Maxwell–Boltzmann distributed velocities and measuring the fraction of trajectories that end in B before A. Simulations have been performed for $x,y \in [-2, 2]$ on a 80×80 grid ($\Delta x = \Delta y = 0.05$). The (inverse) temperature was set to $\beta \equiv (k_B T)^{-1} = 2.5$, where k_B denotes Boltzmann’s constant, the friction to $\gamma = 2.5$, and the time-step to $\Delta t = 0.1$. For each grid, point trajectories were initiated in blocks of 100 until the error in p_B was less than 1% (between 1500 and 2800 trajectories). The result is shown in Fig. 3. From this result, it follows that the $p_B=0.5$ surface is approximated by $y=2.2x$ around the transition state.

2. One-way shooting point ensemble

The aimless shooting algorithm was developed to create a TPS path ensemble in which the shooting point ensemble stays within the transition state region. However, the aimless shooting algorithm¹² is less suitable for diffusive dynamics on a rough energy surface, in which one might prefer to use the one-way shooting algorithm.³⁰ Moreover, as aimless shooting will focus the shooting point ensemble close to the transition state, it cannot give information about the entire transition (see also Appendix B). Here, we perform TPS using the flexible path length, one-way shooting algorithm for stochastic dynamics.¹⁴ This shooting point ensemble is shown in Fig. 4, together with the minimum energy pathway (MEP).

3. Linear likelihood maximization in a restricted ensemble

We applied the standard linear likelihood maximization¹² on the one-way shooting point set. The results are shown in Fig. 5. In contrast to the aimless shooting algorithm, this shooting point ensemble has contributions over the entire potential, including points close to the initial and final states. However, using the entire set (gray points in Fig. 5) in a linear approximation to the RC leads to the very poor estimate $r=0.03-0.09x+0.44y$ (the dividing surface $p_B=0.5$, corresponding to $r=0$, is shown as a gray line in Fig. 5) because the tails of the shooting point distribution have a strong influence on the placement of the optimal dividing surface. Clearly, this is caused by the nonlinearity of the mechanism in this potential. Restricting the shooting point ensemble by, e.g., taking only points within a certain distance from the $r=0$ line (shown as an orange ensemble), im-

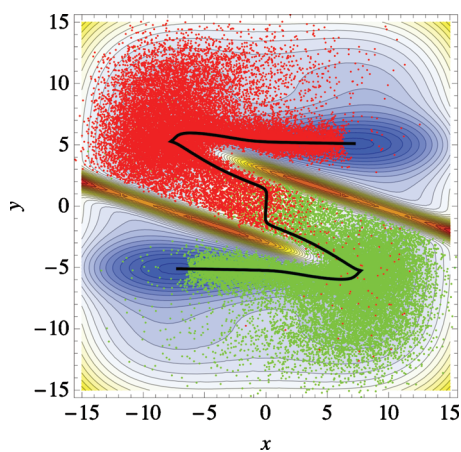


FIG. 4. The shooting point ensemble obtained from a TPS simulation, employing the one-way shooting algorithm plotted onto the z-potential. Green and red points indicate shots that end in A and B , respectively. The MEP is plotted as well, for clarity.

proves the RC estimate to $r=0.05-0.25x+0.20y$ (the $r=0$ line is shown in orange), but still does not resemble the correct dividing surface shown in Fig. 3. Only when restricting the shooting points ensemble even more (blue ensemble) could we recover the correct RC $r=0.06-0.27x+0.11y$ for the transition state region (cf. Fig. 3). From this exercise it follows that (1) a linear RC approximation does not work very well for nonlinear mechanisms such as the z-potential; (2) because of the lack of a well described criterion, the restriction procedure of the one-way shooting point ensemble to the transition state area is arbitrary; and (3) while the correct RC of Fig. 3 describes the dividing surface in the transition state region, it is not capable of describing the entire transition. In Sec. III C we will employ the nonlinear string RC. To obtain the required accuracy for the shooting ensemble in the tails, we will make use of the RPE.

C. String optimization for the RPE

1. The RPE using linear interfaces

We obtained the data points for the string optimization from a RETIS simulation in the z-potential using linear in-

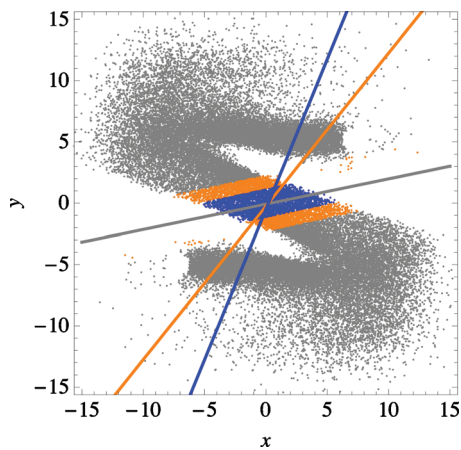


FIG. 5. The effect of cutting the ensemble on the RC optimization. The gray points and line depict the entire shooting point ensemble. The gray line is the optimal linear dividing surface $r=0$. Restricting the ensemble to the yellow points improves the RC somewhat, but only for the blue ensemble is the correct dividing surface recovered.

terfaces, as described in Ref. 21. In this simulation, the Langevin friction is set to $\gamma=1$, the inverse temperature is $\beta=4$, and the time-step is set to $\Delta t=0.05$. The outcome is a path ensemble for each interface. We store one pathway every 100th shooting moves. For each path only one configuration per ten time-steps is stored. This yields 2800 paths with in total $N_f=1\ 363\ 128$ data points. All these data points contribute to the reweighted path ensemble. The total weight of the RPE, the number to be used in the BIC, is $N_d=e^{22.43}$. The weights for each path can be obtained from a WHAM analysis of the RETIS crossing probability histograms.²¹ As the minimum weight of a path in the RPE is 1, we renormalized the lowest WHAM weight to unity. Note that the thus obtained RPE is only an approximation for the true unbiased path ensemble.

We initialized the string by a linear interpolation (a diagonal) between the stable states. Keeping the end points fixed in the stable state minima, we optimize the string by moving the images perpendicular to the string and accepting or rejecting the move according to an annealing scheme based on the likelihood (cf. Appendix A). The initial likelihood for the diagonal string is around $\ln \mathcal{L}=-4 \times 10^8$; the maximized one was $\ln \mathcal{L}=-4.30820 \times 10^5$. The string corresponding to this optimal likelihood is plotted in Fig. 6. The precise values of these logarithmic likelihoods do not have a direct meaning since they depend on the number of included data points. To show the quality of the fit, the optimized $\ln p_A(\sigma)$ and $\ln p_B(\sigma)$ functions are shown together with the optimized $r(\sigma)$ function in Fig. 6. In the same figure, we show the projected $\ln p_A(\sigma)$ and $\ln p_B(\sigma)$ functions of the shooting point data. The agreement between the data and the fit is good.

2. The RPE from RETIS using the optimized string

In the next step we use the optimized string from Fig. 6 itself to perform a RETIS simulation. The description of the simulation can be found in Ref. 21. Using the same analysis as above, we computed the crossing histograms and applied WHAM. Using the resulting reweighted path ensemble we optimized the string starting from a diagonal interpolation between A and B . For the $N_f=1\ 351\ 929$ points, the initial likelihood for the diagonal string is around $\ln \mathcal{L} \approx -5 \times 10^8$; the maximized one is $\ln \mathcal{L}=-6.502 \times 10^5$. Again, the absolute values of the logarithmic likelihoods do not have direct meaning. Note that the optimized likelihood is in fact lower than it is for the linear interfaces. However, the fit to the data points is much better as is clear from Fig. 7. The final optimized string is also shown in Fig. 7. Note that starting from the stable state, the string points somewhat toward the high energy barriers, but then avoids these. While the optimized string exhibits qualitatively the correct shape of the potential, it does not exactly follow the MEP. This can be due to the fact that the optimization tries to prevent that points would be assigned to the wrong part of the string, leading to strings that move close to the high barrier region.

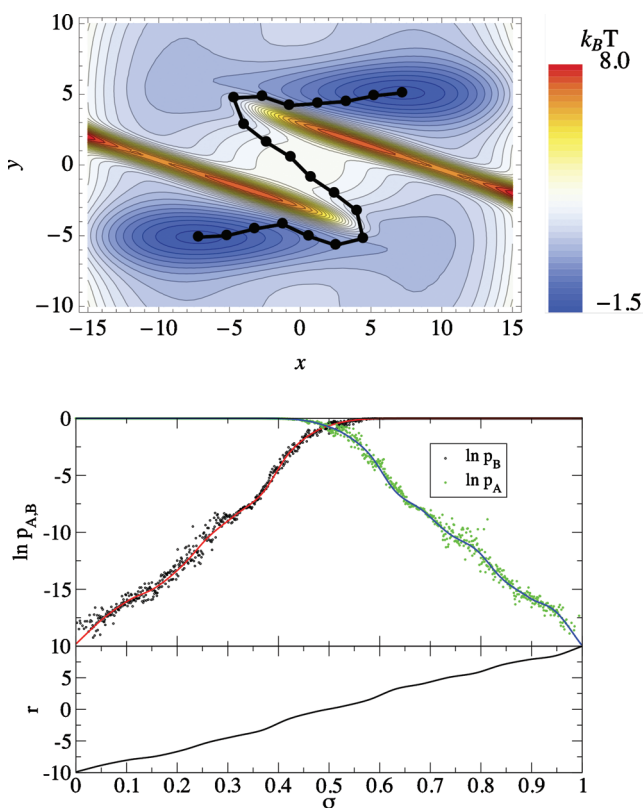


FIG. 6. Top: The optimal string in the z-potential for the RPE using the linear interfaces. Note that the string is close to the high potential barrier regions. Bottom, top panel: The logarithm of $p_B(\sigma)$ (black and red) and $p_A(\sigma)$ (green and blue). The red and blue solid curves denote the model; the black and green points are the data. Lower panel: The parametrization of $r(\sigma)$ by a monotonic cubic spline.

3. Optimizing the number of string images

Subsequently, we optimize the likelihood as a function of the number of string images M . The number of string images could become much lower than 20 images, yielding a string that is not smooth. Because the geometric projection method requires such a smooth string, we use the Voronoi construction together with the linear interpolation of the $r(\sigma)$ mapping (see Sec. II). In this case, reparametrization of the string is not necessary, as the condition of equidistant string points is not required for the Voronoi construction. As the optimization turns out to be computationally more expensive than the projection method, we reduce the data set by a factor of 10. For this situation, the BIC states that the quantity to optimize is $C_{\text{BIC}} = \ln \mathcal{L} - \frac{3}{2}M \ln N_d$.

Starting with three images on the string, keeping the first and last images fixed, we compute the optimal likelihoods as a function of string image number by the MC annealing scheme (see Appendix A). New points are added to the string by linear interpolation. Figure 8 shows the optimized $\ln \mathcal{L}$ as a function of string images for the linear interfaces RPE. Also plotted in the same figure is the penalty $\frac{3}{2}M \ln N_d^{\text{lin}} + \text{const}$ that needs to be overcome according to the BIC (straight line) with an arbitrary constant. Here, $\ln N_d^{\text{lin}} = 22.43$. The top panel shows the difference between these two, expressed by C_{BIC} , shifted such that the maximum is zero.

Going from $M=3$ to $M=4$ increases the logarithmic

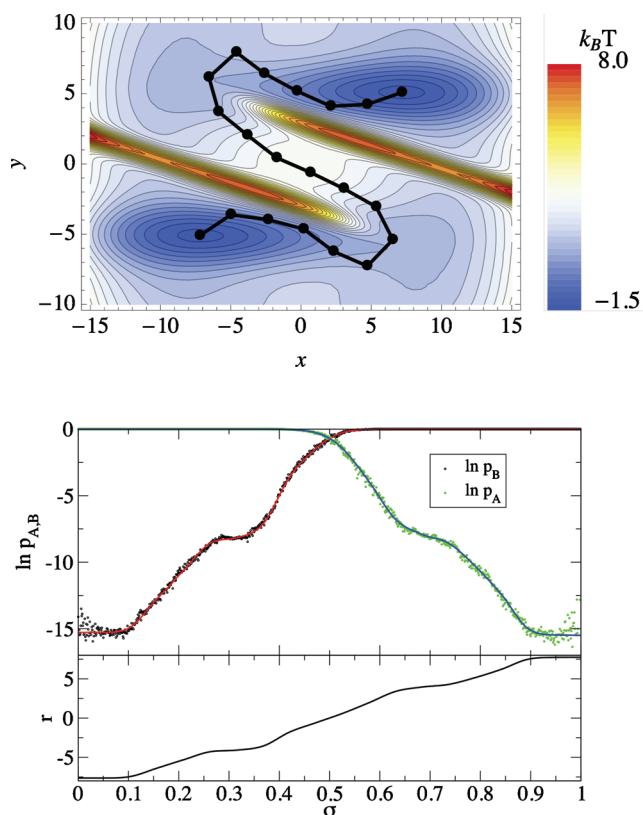


FIG. 7. Top: The optimal string in the z-potential for the RPE using the optimized string shown in Fig. 6. Note that the string now avoids the high potential region. Bottom, top panel: The logarithm of $p_B(\sigma)$ (black and red) and $p_A(\sigma)$ (green and blue). The red and blue solid curves denote the model; the black and green points are the data. Bottom, lower panel: the parametrization of $r(\sigma)$ by a monotonic cubic spline.

likelihood from $\ln \mathcal{L} = -3.5 \times 10^7$ to $\ln \mathcal{L} = -4.3225 \times 10^4$. The optimized string for $M=4$ already has the shape of the letter Z. Adding more string points does improve the logarithmic likelihood, but is not significant enough according to the BIC. This is clear from the top panel in Fig. 8, where the maximum is indeed at $M=4$.

We repeat this exercise for the RPE obtained through the optimized string (see Fig. 9). Here, $\ln N_d^{\text{str}} = 21.45$. In this case, C_{BIC} is maximal for $M=6$. The optimal string is plotted in Fig. 10. Apparently in this case, adding two points to the minimum $M=4$ does improve the likelihood significantly, as is visible from the C_{BIC} plot in the top panel. Adding a string point close to the origin is much less useful. When adding more points, the string does improve, but not enough, according to the BIC. Interestingly, the $M=6$ string in Fig. 10 is already very similar to the optimized 20 image string of Fig. 7. Starting from the initial state, the RC first roughly points into the direction of the final state, but has to make a detour because of the two high barrier ridges. Also, note that while the RC roughly follows the shape of the potential, it is not identical to the minimum (free) energy pathway.

D. What is the best collective variable space?

In our case it is clear that a 2D string in the x, y plane will describe the reaction coordinate for the z-potential better than any description using only x or y . However, to complete

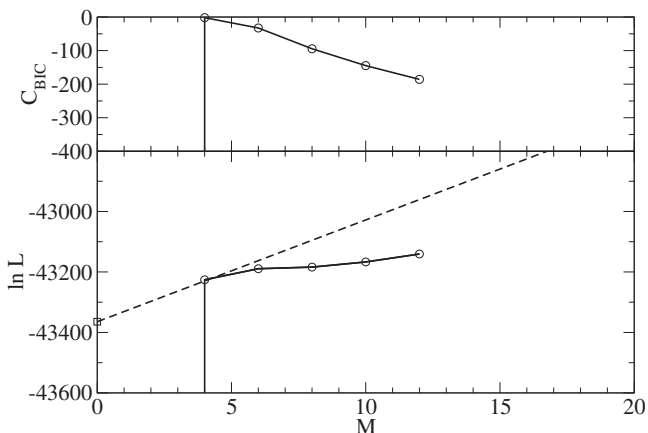


FIG. 8. Lower panel: Logarithmic likelihood as a function of the string image number M based on the linear interfaces RPE and using the Voronoi projection. Starting with four points, new strings are created by adding one or more points by interpolation. The penalty term $-1.5M \ln N_d$ as a function of the string image number M is given by the dashed line. Top panel: C_{BIC} shifted such that the maximum is at zero.

the analysis, we will also optimize the likelihood for the 1D cases. This is simply done by projecting all the RPE points to either the x -axis or the y -axis and maximizing the likelihood by optimizing the $r(\sigma)$ curve with 20 points. For the RPE based on the optimized string RETIS, the result is for x only $\ln \mathcal{L} = -1.7 \times 10^8$, giving a $C_{\text{BIC}} = \ln \mathcal{L} - 10 \ln N_d^{\text{str}} \approx -1.7 \times 10^8$. Here $\ln N_d^{\text{str}} = 23.76$ is larger than in Sec. III C because there are ten times more path points. The maximization for y yields $\ln \mathcal{L} = -2.5 \times 10^7$ and a $C_{\text{BIC}} = \ln \mathcal{L} - 10 \ln N_d^{\text{str}} \approx -2.5 \times 10^7$. Based on this, it follows that y as a reaction coordinate is far better than x alone, although it is clearly not capable of describing the reaction. In the 2D case, the diagonal $y=x$ results in a value of $\ln \mathcal{L} = -5 \times 10^8$; in contrast, the optimized string gives $\ln \mathcal{L} = -6.50200 \times 10^5$ with a $C_{\text{BIC}} = \ln \mathcal{L} - 30 \ln N_d^{\text{str}} = \ln \mathcal{L} - 712 \approx -6.5 \times 10^5$, an improvement of almost three orders of magnitude in logarithmic likelihood. Hence we can conclude that for the z-potential, the string description in x, y space is most appropriate, as ex-

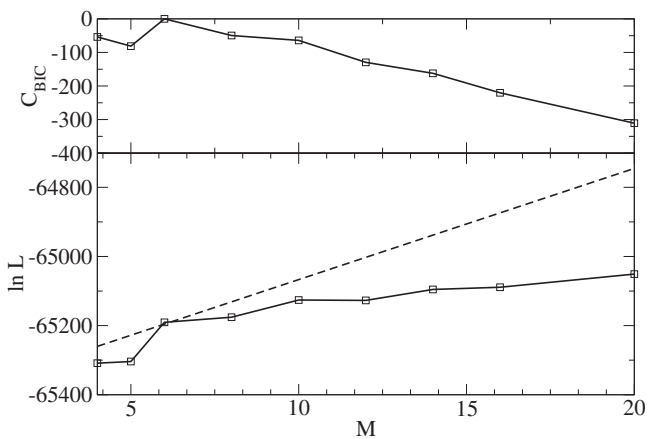


FIG. 9. Lower panel: Logarithmic likelihood as a function of the string image number M based on the string RPE and using the Voronoi projection. Starting with four points, new strings are created by adding one or more points by interpolation. The penalty term $-1.5M \ln N_d$ as a function of the string image number M is given by the dashed line. Top panel: C_{BIC} shifted such that the maximum is at zero.

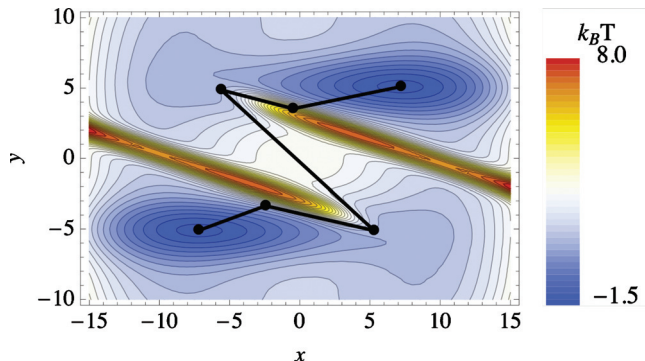


FIG. 10. Optimized string description for $M=6$ in the z-potential.

pected. However, in the general case of a complex reaction, the choice of parameters is not as clear. In that case, the likelihood maximization provides a quantitative measure to distinguish between different choices of collective variables.

IV. CONCLUSIONS

We have presented a novel optimization method for obtaining a nonlinear RC described by a string. Based on the LM analysis of Peters and Trout and concepts from the string method of Vanden-Eijnden and co-workers, the approach gives the best stringlike description of the RC in a low dimensional space of collective variables. Moreover, the analysis yields a description of the reaction of interest, not only around the TS region but along the entire reaction pathway. As such, the method can be used to extract the essential dynamical features from the collection of many pathways. The presented approach requires the complete unbiased path ensemble, which can, in principle, be obtained by regular MD, but much more efficiently by a path sampling method for the rare events we consider here. We have shown previously how to use the replica exchange TIS to obtain the reweighted path ensemble.²¹ Using the RPE as an estimate for the unbiased path ensemble, we optimize the string description of the RC as a function of the number of string images, as well as a function of the number of collective variable dimensions. The string-LM method can be applied iteratively: a first guess of the RC can be used to define the TIS interfaces. After applying the LM, the optimal string can then be used as a new set of interfaces to obtain a new RPE from the RETIS, which can then be reanalyzed. Convergence of the RC ensures that one has sampled correct pathways and, moreover, has found the correct description of the reaction.

While our method is strongly related to the string method in collective variable space,^{20,31} a major difference is the way that the information about the committor is computed. Another important difference is that our method provides a means to determine which collective variables to choose from a single sampling of the RPE. In the string method, comparing different collective variable spaces would require different string optimizations.²⁰

The RC optimization as it is proposed here is based on a nonlinear fitting to the committor. In the TPT framework, the definition of the probability current of reactive trajectories is

an important concept that contains much information on the mechanism.^{6,7} In fact, it is stated in Refs. 6 and 7 that the probability current is a better way to characterize the mechanism than the committor, as it is not influenced by “dead ends.” In principle, it should be possible to use this probability current to optimize the reaction mechanism using a non-linear reaction coordinate. However, this would require a different, yet unknown, definition of the likelihood function.

We envision that the approach advocated in the current work can lead to new insights in the reaction coordinates of very complex processes, including protein folding, and crystal nucleation. In a future study, we aim to apply our method to the nucleation of crystals.

ACKNOWLEDGMENTS

P.G.B. thanks Eric Vanden-Eijnden and Baron Peters for fruitful discussions. This work was financially supported by the “Nederlandse Organisatie voor Wetenschappelijk Onderzoek (NWO)” and the “Stichting Nationale Computerfaciliteiten” (NCF).

APPENDIX A: ANNEALING PROCEDURE

The string can be optimized by a Monte Carlo annealing method. In this algorithm, the string images are moved randomly in the collective variable space and accepted or rejected based on the difference in likelihood. The acceptance criterion is

$$P_{\text{acc}} = \min[1, \exp(\beta \Delta \ln \mathcal{L})], \quad (\text{A1})$$

where $\Delta \ln \mathcal{L}$ is the difference in logarithmic likelihood caused by the move of the image and β is an artificial temperature. In the current work, $\beta=1$ initially and subsequently is slowly decreased. We employ two annealing schemes, based on whether we use the geometrical projection methods²¹ or the Voronoi construction. In the first case, we move the trial image perpendicular to the string. Because the projection method requires equidistant string images, we apply the reparametrization scheme of the string method.¹⁹ Then, the monotonic spline $r(\sigma)$ mapping is optimized, by a second annealing algorithm, working in the same way. This part of the optimization is accelerated by precomputing the $p_B(\sigma)$ histograms because then the likelihood can be expressed as a sum over the histogram, rather than over all points in the ensemble.

For the case of the Voronoi construction, we opt for the simultaneous optimization, graphically depicted in Fig. 1. Here we move randomly a string image or a σ point. The advantage is that all the variables are treated on the same level. The down side is that each move requires a Voronoi projection of all points in the RPE.

APPENDIX B: PROPERTIES OF THE SHOOTING POINT ENSEMBLE

The distribution of points used for the likelihood maximization of the committor function is crucial for the estimation of the RC. In this appendix, we elucidate the properties of the shooting point distribution (or shooting point ensemble) of various shooting algorithms in comparison to the

distribution from the RPE and its impact on the likelihood function. As an illustrative example, we will use a model that consists of a single particle in a finite one-dimensional external potential

$$v(x) = \epsilon \frac{a^2 - (a-x)^2}{a^2}. \quad (\text{B1})$$

Here, x is the position of the particle, a is the position of the maximum of the quadratic potential, and ϵ sets the energy scale. For simplicity, the position can only take values within the interval $0 \leq x \leq 2a$. This simple model serves as a general example for a system with a free energy barrier separating two stable states. For this system, the committor function can be evaluated analytically using the backward Kolmogorov equation^{31,32} which simplifies in this case to

$$\frac{\partial \beta v(x)}{\partial x} \frac{\partial p_B}{\partial x} = \frac{\partial^2 p_B}{\partial x^2}. \quad (\text{B2})$$

With the boundary conditions $p_B=0$ for $x=0$ and $p_B=1$ for $x=2a$, the solution is

$$p_B(x) = \frac{1}{2} \left(1 + \frac{\text{erf}\left(\frac{x-a}{a}\sqrt{\beta\epsilon}\right)}{\text{erf}(\sqrt{\beta\epsilon})} \right), \quad (\text{B3})$$

where $\beta\epsilon$ plays the role of a dimensionless reduced inverse temperature. With an analytic expression for p_B , we can also calculate the distribution of the trial shooting points P_{trial} and a subset of these, the accepted shooting points P_{acc} , i.e., shooting points that result in trajectories that are accepted. In a two-way shooting simulation, a shooting point is accepted with a probability $P_{\text{acc}}=2P(x|\text{TP})p_A p_B$ and rejected with a probability $P_{\text{rej}}=P(x|\text{TP})(p_A^2+p_B^2)$. Here, $P(x|\text{TP})$ is the probability to choose a certain shooting point x from a transition path TP. The trial shooting points are the sum of accepted and rejected points: $P_{\text{trial}}=P_{\text{acc}}+P_{\text{rej}}=P(x|\text{TP})$, where we used $p_A+p_B=1$. Applying the relation $P(x|\text{TP})P(\text{TP})=P(\text{TP}|x)P(x)$ (Ref. 10), we find that

$$P_{\text{trial}}^{\text{TPS}} \propto p_B p_A e^{-\beta v(x)}. \quad (\text{B4})$$

Here, we have used that $P(\text{TP})$ is a constant and $P(x)$ is the Boltzmann distribution. The accepted shooting points are distributed according to

$$P_{\text{acc}}^{\text{TPS}} \propto 2P(x|\text{TP})p_A p_B = p_B^2 p_A^2 e^{-\beta v(x)}. \quad (\text{B5})$$

The approach of aimless shooting is to focus on shooting points that are actually accepted by biasing the shooting toward the transition state. These shooting points result in trajectories that are accepted or rejected considering the usual TPS acceptance criterion. The trial shooting points are simply the sum of rejected and accepted shooting points, where we find that the distribution of rejected shooting points $P_{\text{rej}}^{\text{aimless}}$ is broader than the distribution of accepted shooting points $P_{\text{acc}}^{\text{aimless}}$ because the probability of rejecting a shooting move increases with the distance of the shooting point with respect to the transition state. However, the distribution of the trial shooting points as well as $P_{\text{acc}}^{\text{aimless}}$ and $P_{\text{rej}}^{\text{aimless}}$ are peaked at the transition state.

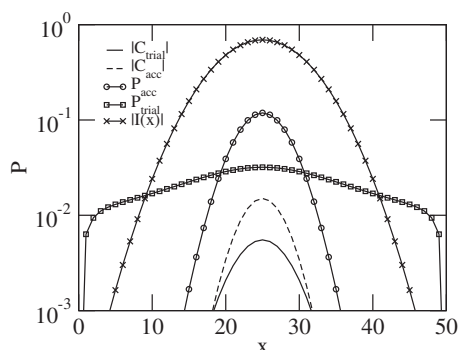


FIG. 11. Analytic result for the contributions to the likelihood function for $a=25$ and $\beta\epsilon=10$. For the trial distribution $P_{\text{trial}}^{\text{TPS}}$ (squares), the contribution $C_{\text{trial}}=I(x)P_{\text{trial}}^{\text{TPS}}$ (solid line) is strongly peaked around the transition state at $x=25$. This peak is even more pronounced for $P_{\text{acc}}^{\text{TPS}}$ (circles) which leads to a contribution function C_{acc} (dashed line). Note that the ensemble of trial shooting points from aimless shooting is equivalent to P_{acc} and that of one-way shooting is equivalent to P_{trial} . The absolute values of $C(x)$ and $I(x)$ are plotted for comparison on a logarithmic scale.

For one-way shooting, the probability to accept a forward shot is $P_{\text{acc},\text{for}}=\frac{1}{2}P(x|\text{TP})p_B$; the probability for a backward shot is $P_{\text{acc},\text{back}}=\frac{1}{2}P(x|\text{TP})p_A$. The factor 1/2 comes from the fact that we choose a forward or a backward shot with the same probability. Combining the two, we find that the overall distribution of accepted shooting points is $P_{\text{acc}}^{\text{oneway}}=\frac{1}{2}P(x|\text{TP})$. Similarly, the distributions of the rejected shooting points are $P_{\text{rej},\text{for}}=\frac{1}{2}P(x|\text{TP})p_A$ and $P_{\text{rej},\text{back}}=\frac{1}{2}P(x|\text{TP})p_B$. This means for one-way shooting, the trial shooting points, the accepted shooting points, as well as the rejected shooting points all share the same distribution $P(x|\text{TP})$.

These distributions are the basis for the likelihood estimation. However, the accuracy is not simply related to this relation because the particular form of the likelihood introduces an intrinsic weight for points close to the transition state. This means that even if the points would be drawn uniformly over the whole transition, only the ones close to the transition state would actually contribute to the likelihood. This is best seen by rewriting the likelihood function for the perfect fit $p_B^{\text{est}}=p_B$.

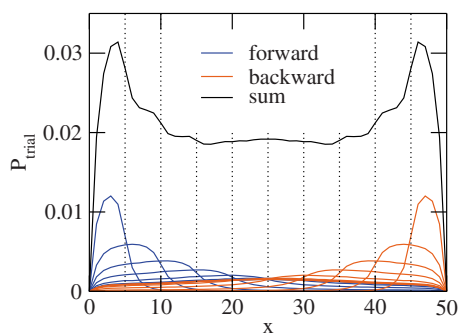


FIG. 12. Distribution of the trial shooting points in a TIS simulation with nine interfaces at positions indicated by the dotted lines. The normalized overall distribution (black) is the sum of all forward (blue) and backward (red) trajectories.

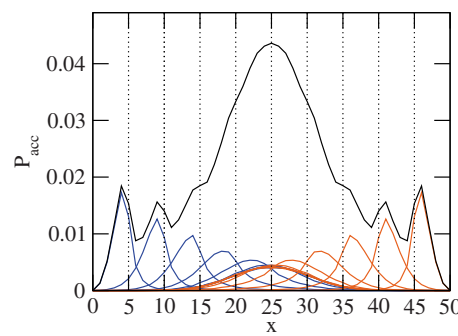


FIG. 13. Distribution of the accepted shooting points from the TIS simulation. The color code is that same as in Fig. 12.

$$\begin{aligned}\ln \mathcal{L} &= \sum_{x \rightarrow B} \ln(p_B(x)) + \sum_{x \rightarrow A} \ln(1 - p_B(x)) \\ &= N \left[\sum_x P(x)p_B(x) \ln p_B(x) + \sum_x P(x)p_A(x) \ln p_A(x) \right] \\ &= N \sum_x P(x)[p_B(x) \ln p_B(x) + p_A(x) \ln p_A(x)].\end{aligned}\quad (\text{B6})$$

In the second line, we have used the fact that we can rewrite the sum over all $x \rightarrow B$ as the sum over all x of the probability that x ends up in B . This is the probability of generating x [i.e., $P(x)$] times the probability that this point will lead to a trajectory that ends in B (i.e., p_B). The number of points N can be taken out of the sum. Analogous for points that end in A in the third line, where we have also used $p_A=1-p_B$. The second term in the sum is an intrinsic weight of the likelihood function and because of its particular form, we will refer to it in the following as information weight $I(x)=p_B(x)\ln p_B(x)+p_A(x)\ln p_A(x)$. The individual contributions of each point x to the sum are therefore denoted as $C(x)=P(x)I(x)$. We will now study the contribution function for different distributions $P(x)$ depicted in Fig. 11. The trial shooting points of aimless shooting are distributed according to P_{acc} and the trial shooting points of one-way and two-way shooting are distributed according to P_{trial} . In both cases, only shooting points close to the transition state contribute to the likelihood function. The shooting point distributions in a TIS simulation depend on the particular choice of the positions of the interfaces and cannot be written as an ana-

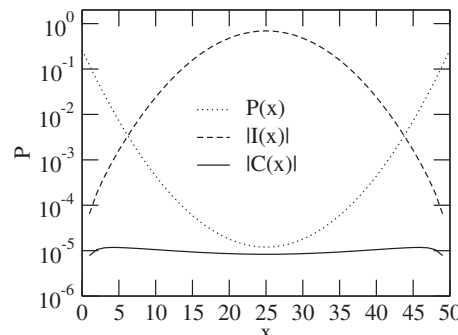


FIG. 14. Contribution function for data points taken from the reweighted path ensemble which are distributed according to their Boltzmann factor (dotted line). Multiplied with the information weight $I(x)$ (dashed line), the contributions to the likelihood becomes a flat line (solid). For comparison, the absolute values of $I(x)$ and $C(x)$ are plotted.

lytic function. Therefore, we employ a Monte Carlo simulation with interfaces at the positions $x=5, 10, 15, 20, 25, 30, 35, 40, 45$ to estimate these distributions. Trajectories are generated with a procedure where the particle is attempted to move at random from x_o to x_n at each step with an acceptance probability of $\text{acc}(o \rightarrow n) = \min[1, \exp(-\beta(v(x_n) - v(x_o)))]$. The resulting shooting point ensembles of the accepted and trial shooting points are shown in Figs. 12 and 13, respectively. Here, the distribution of the trial shooting points is almost uniform over the whole transition. Clearly, multiplying a flat distribution with the information function $I(x)$ leads to a contribution of points only at the transition state. This means that a likelihood maximization based on the TIS shooting point ensemble would not be sufficient to describe the whole transition.

However, the reweighted path ensemble shows a different picture. The distribution of points becomes simply the Boltzmann distribution: $P(x) \propto e^{-\beta\Delta F(x)}$. This is a function with two strong peaks at the stable states and a minimum at the transition state, in contrast to the function $I(x)$ which is peaked around the transition state and vanishes close to A and B . These two factors cancel each other to a large degree and the contributions to the likelihood becomes almost uniform over the whole range from state A to state B (see Fig. 14). Clearly, the product of the Boltzmann factor and the information weight from the likelihood lead to an almost flat contribution function. This means the information that goes into the likelihood estimation is uniform over the whole transition, only if the full path ensemble is taken into account.

Remarkably, in Eq. (B6), we have assumed that we found the perfect estimate for p_B ; the likelihood, however, does not vanish but rather becomes a constant times the number of data points. This can be considered as the upper limit for the given distribution. In the case of this simple model, we can explicitly calculate the sum in Eq. (B6) because the normalization factor Z in the Boltzmann weight is known when we assume that phase space is restricted to only points between A and B . Then the upper limit for the maximum likelihood is $\max[\ln \mathcal{L}]^* = N \sum_x P(x) / Z I(x)$

$= -0.00048N$, with N as the number of data points. In the RPE this number is $N = N_d \equiv \sum_{i=0}^{N_f} \omega_i$, where N_f is the number of time slices in the path ensemble.

- ¹G. M. Torrie and J. P. Valleau, *Chem. Phys. Lett.* **28**, 578 (1974).
- ²E. Carter, G. Ciccotti, J. T. Hynes, and R. Kapral, *Chem. Phys. Lett.* **156**, 472 (1989).
- ³A. Laio and M. Parrinello, *Proc. Natl. Acad. Sci. U.S.A.* **99**, 12562 (2002).
- ⁴C. Dellago, P. G. Bolhuis, and P. L. Geissler, *Adv. Chem. Phys.* **123**, 1 (2002).
- ⁵C. Dellago, P. G. Bolhuis, F. S. Csajka, and D. Chandler, *J. Chem. Phys.* **108**, 1964 (1998).
- ⁶W. E and E. Vanden-Eijnden, *J. Stat. Phys.* **123**, 503 (2006).
- ⁷W. E and E. Vanden-Eijnden, *Annu. Rev. Phys. Chem.* **61**, 391 (2010).
- ⁸P. G. Bolhuis, C. Dellago, and D. Chandler, *Proc. Natl. Acad. Sci. U.S.A.* **97**, 5877 (2000).
- ⁹A. Ma and A. R. Dinner, *J. Phys. Chem. B* **109**, 6769 (2005).
- ¹⁰G. Hummer, *J. Chem. Phys.* **120**, 516 (2004).
- ¹¹R. Best and G. Hummer, *Proc. Natl. Acad. Sci. U.S.A.* **102**, 6732 (2005).
- ¹²B. Peters and B. L. Trout, *J. Chem. Phys.* **125**, 054108 (2006).
- ¹³B. Peters, G. T. Beckham, and B. L. Trout, *J. Chem. Phys.* **127**, 034109 (2007).
- ¹⁴J. Juraszek and P. G. Bolhuis, *Biophys. J.* **95**, 4246 (2008).
- ¹⁵J. Vreede, J. Juraszek, and P. G. Bolhuis, *Proc. Natl. Acad. Sci. U.S.A.* **107**, 2397 (2010).
- ¹⁶E. Borrero and F. Escobedo, *J. Chem. Phys.* **127**, 164101 (2007).
- ¹⁷G. T. Beckham, B. Peters, C. Starbuck, N. Variankaval, and B. L. Trout, *J. Am. Chem. Soc.* **129**, 4714 (2007).
- ¹⁸B. Pan, M. S. Ricci, and B. L. Trout, *J. Phys. Chem. B* **114**, 4389 (2010).
- ¹⁹W. E, W. Ren, and E. Vanden-Eijnden, *Phys. Rev. B* **66**, 052301 (2002).
- ²⁰E. Vanden-Eijnden and M. Venturoli, *J. Chem. Phys.* **130**, 194103 (2009).
- ²¹J. Rogal, W. Lechner, J. Juraszek, B. Ensing, and P. G. Bolhuis, *J. Chem. Phys.* **133**, 17109 (2010).
- ²²J. Juraszek and P. G. Bolhuis, *Proc. Natl. Acad. Sci. U.S.A.* **103**, 15859 (2006).
- ²³J. Langer, *Ann. Phys.* **54**, 258 (1969).
- ²⁴A. Berezhkovskii and A. Szabo, *J. Chem. Phys.* **122**, 014503 (2005).
- ²⁵T. S. van Erp, D. Moroni, and P. G. Bolhuis, *J. Chem. Phys.* **118**, 7762 (2003).
- ²⁶A. M. Ferrenberg and R. H. Swendsen, *Phys. Rev. Lett.* **63**, 1195 (1989).
- ²⁷T. S. van Erp, *Phys. Rev. Lett.* **98**, 268301 (2007).
- ²⁸P. G. Bolhuis, *J. Chem. Phys.* **129**, 114108 (2008).
- ²⁹G. Schwarz, *Ann. Stat.* **6**, 461 (1978).
- ³⁰P. G. Bolhuis, *J. Phys.: Condens. Matter* **15**, S113 (2003).
- ³¹L. Maragliano, A. Fischer, E. Vanden-Eijnden, and G. Ciccotti, *J. Chem. Phys.* **125**, 024106 (2006).
- ³²P. Metzner, C. Schütte, and E. Vanden-Eijnden, *J. Chem. Phys.* **125**, 084110 (2006).